STRESS BRIDGING IN PARTICULATE COMPOSITES AND CALCULATION OF G_{23} IN PARTICULATE COMPOSITES

by

Gopal Narra

A thesis submitted to the faculty of
The University of Utah
in partial fulfillment of the requirements for the degree of

Master of Science

Department of Mechanical Engineering

The University of Utah

May 2012

The University of Utah Graduate School

STATEMENT OF THESIS APPROVAL

The thesis of **Gopal Narra**

has been approved by the following supervisory committee members:

Daniel O. Adams	, Chair	**12/21/2011** Date Approved
K.L. DeVries	, Member	**12/21/2011** Date Approved
Ken Monson	, Member	**12/21/2011** Date Approved

and by **Timothy A. Ameel** , Chair of the Department of **Mechanical Engineering**

and by Charles A. Wight, Dean of The Graduate School.

ABSTRACT

High energy materials are commonly used as solid rocket motors propellants. The properties of HE materials can be determined experimentally; however, the hazards associated with experiments on these materials, as well as the costs, make this approach unattractive. The simulations of these materials require techniques that can bridge submicron scales and engineering scales. Micromechanics provides such techniques. The objective of this research is to investigate the effects of stress bridging on predicting the effective properties of high energy materials group. The research focused on polymer bonded explosives (PBXs), since detailed numerical simulations of PBXs are computationally expensive. The generalized method of cells was explored for this research and its predictions of elastic moduli with and without stress bridging.

The results show that stress bridging affects the estimated properties considerably. The generalized method of cells without stress bridging is shown to underestimate the elastic moduli of the polymer bonded explosives.

Micromechanics analysis requires that the fundamental material properties of the constituents are known initially. The composite material properties can be determined experimentally by testing actual composite specimens. However, in recent years, more and more attention has been given to the development of the analytical and numerical models for predicting composite material properties from the properties of the constituent materials and their relationship to each other. The other part of this research is to identify the Representative Volume Element (RVE) and the boundary conditions for calculation of transverse shear modulus (G_{23}) and then compare the results to the other classical micromechanics solutions.

The results show that the proposed approach for identifying the Representative Volume Element (RVE) and the boundary conditions predict as accurately as the other classical micromechanics solutions.

To Mom, Dad and Dear Wife Pratima.

CONTENTS

LIST OF FIGURES

LIST OF TABLES

ACKNOWLEDGEMENTS

First and foremost, I would like to gratefully acknowledge the supervision of my advisor, Dan Adams, during this work. I will always be indebted to Dan Adams for being supportive of me and my work. I would like to thank The University of Utah Center for the Simulation of Accidental Fires and Explosions(C-SAFE) for funding this research. Finally, I am forever indebted to my parents and Pratima for their understanding, endless patience and encouragement when it was most required.

CHAPTER 1

INTRODUCTION

1.1 Composites

A composite material as the name suggests is composed of two or more materials. The general idea of combining several components is to produce a material with properties that are different from the individual components themselves. A simple example of a composite would be concrete. Concrete is made up of cement, sand, stones, and water. A properly designed composite can offer significant advantages in strength, stiffness, light weight, relative to conventional metallic materials.

Composites are typically classified into two main groups. The first group of composites are called the filled materials. These composites are based on matrix material. The properties of the matrix are improved by filling it with particles. This group consists of the Metal Matrix Composites (MMC), Ceramic Matrix Composites (CMC), and Polymer Matrix Composites (PMC). The second group is called reinforced materials. These composites are sometimes referred as the advanced composites. The basic components of these materials are long and thin fibers bound in a matrix material. The matrix holds the reinforcement to form the desired shape while the reinforcement improves the overall mechanical properties of the matrix. This group consists of Particulate Composites, Fibrous Composites and Laminate Composites.

Fiber reinforced composites are composed of fibers and a matrix. Fibers are the reinforcement and the main source of strength while the matrix glues all the fibers together in shape and transfers stresses between the reinforcing fibers. The primary function of the matrix is to transfer stresses between the reinforcing fibers (hold fibers together) and protect the fibers from mechanical and/or environmental damages. A basic requirement for a matrix material is that its strain at break must be larger than

the fibers it is holding. Most matrices are made of resins for their wide variation in properties and relatively low cost. Sometimes, fillers or modifiers might be added to smooth manufacturing process, impart special properties, and/or reduce product cost.

1.2 High Energy Materials

High-energy (HE) materials are commonly used as solid rocket motors propellants. Interest in the mechanical properties of HE materials has developed with improvements in computational capabilities that make possible simulations of containers filled with these materials. Though mechanical properties of HE materials can be determined experimentally, the hazards associated with experiments on these materials, as well as the attending costs, make this option unattractive. Improved numerical and computational techniques make the determination of mechanical properties of HE materials possible by bridging the gaps between atomistic calculations of molecular potentials, molecular dynamics simulations and micromechanics methods for composite materials. In this research, some micromechanics based methods for the determination of the mechanical properties of composites are explored and applied to a group of HE materials called polymer-bonded explosives (PBXs).

1.3 Thesis Organization

This document contains a review of an admittedly unconventional master's research program. Rather than focusing all attention on a particular area of study, this research program has given attention to two different aspects within the general topic of particulate composites. To facilitate publication of results from specific topics, this thesis has been organized into two main chapters, which are independent documents. These papers are intended for publication in various technical journals; hence each paper contains introduction, discussion, results section, references and figures particular to that paper only.

A review of the properties of polymer bonded explosives and in particular PBX 9501 is provided in Chapter 2. The chapter discusses the effects of stress bridging

in particulate composites. The estimations of effective properties of polymer bonded explosives with stress bridging from generalized method of cells (GMC) are compared to finite element based estimates.

Chapter 3 deals with the estimation of G_{23} in unidirectional composites. A discussion of classical numerical methods of predicting the effective properties of composites is provided. The new approach and the classical solutions are compared for validation.

Finally, Chapter 4 presents a list of general recommendations for the topics discussed in Chapter 2 and Chapter 3.

CHAPTER 2

STRESS BRIDGING IN PARTICULATE COMPOSITES

2.1 Introduction

2.1.1 Polymer-Bonded Explosives

Polymer-bonded explosives (PBXs) are particulate composites containing two or more components. One of the components is an explosive crystal while the other components act as a binder that provides structural support to the crystals. Some PBXs and their components [1, 2, 3] are listed in Table 2.1. It can be observed from the table that all these PBXs contain a very high weight fraction of particles (>90%). The particles are considerably stiffer than the binder at room temperature.

2.1.2 PBX 9501

The polymer-bonded explosive of interest in this research is PBX 9501 because of the availability of experimental data. PBX 9501 is a particulate composite containing crystals of HMX (High Melting Explosive) in a binder composed of Estane 5703 and BDNPA/F. In addition, a free radical inhibitor such as diphenylamine or Irgonox is usually added to the binder [4]. A detailed composition of PBX 9501 is shown in Table 2.2. The small volume fraction occupied by Irgonox can be neglected. The voids occupy only 2% of the volume and are neglected in this research.

The dry blend HMX particles in PBX 9501 are mixed in a 3 to 1 ratio of coarse to fine grades of HMX. The coarse HMX grade particles are sized between 44 and 300 microns while the fine HMX grade particles are less than 44 microns in size. The finer particles fit into the spaces between the larger particles. The large particles occupy most of the volume of the composite.

The manufacture of PBX 9501 involves mixing the dry blend of HMX and the

Table 2.1. Compositions of common PBX materials.

Binder Type	PBX	Explosive/Binder	Weight(%)	Source
Fluoropolymer	LX-10-1	HMX[a]/Viton[b]	95.5/4.5	[1]
(e.g., Viton)	PBX 9502	TATB[c]/KEL-F-800[d]	95/5	[1]
	PBX 9010	RDX[e]/KEL-F-3700[f]	90/10	[2]
	PBX 9407	RDX/Exon-461[g]	94/6	[2]
	PBX 9207	HMX/Exon-461	92/8	[2]
Polyeurethene	PBX 9011	HMX/Estane 5703[h]	90/10	[2]
	EDC 29	HMX/HTPB[i]	95/5	[3]
Polyeurethene	PBX 9404	HMX/NC[j]+CEF[k](1:1)	94/6	[2]
(with	EDC 37	HMX/NC+K10[l](1:8)	91/9	[3]
Plasticizers)	PBX 9501	HMX/ Estane 5703+BDNPA/F[m](1:1)	95/5	[2]

a HMX : 1,3,5,7-tetranitro-1,3,5,7-tetraazacyclooctane
b Viton : random copolymer of hexfluoropropane and vinylidene fluoride (1:2)
c TATB : triaminotrinitrobenzene
d KEL-F-800 : random copolymer of chlorotrifluoroethylene and vinylidene fluoride (3:1)
e RDX : $C_3H_6N_6O_6$
f KEL-F-3700 : $(CFClCF_2CH_2CF_2)_n$
g Exon-461 : $(CFClCF_2CH_2CF_2)_n$
h Estane 5703 : segmented polyeurethene of low molecular weight poly(butylene adipate) soft segments and 4,4 diphenylmethane diisocyanate 1,4 butanediol hard segments.
i HTPB : hydroxyl terminated poly butadiene
j NC : nitrocellulose
k CEF : chloroethyl phosphate
l K10 : plasticizer (composition not known)
m BDNPA/F : bis-dinitropropylacetal/formal

Table 2.2. Weight and volume fractions of the components of PBX 9501.

Component	Weight Fraction	Volume Fraction[a]
HMX	0.9	0.92[b]
Estane 5703	0.025	0.039
BDNPA/F	0.025	0.033
Irgonox	0.001	0.0
Voids	0.0	0.01-0.02

a The volume fraction data have been obtained from Dick et al. [5].
b McAfee et al. [6] cite volume fractions of 0.912 and 0.088 for HMX and binder respectively.

binder to form molding powder granules (prills) of PBX 9501. These powders are then isostatically compressed at 90° C until the porosity is reduced to 1-2% and the pressed form of PBX 9501 is obtained. The microstructure of the pressed PBX9501 [7] is shown in Figure 2.1. The size distribution of HMX particles in PBX 9501 after processing is significantly different from that before processing. Experiments by Skidmore et al. [8] have shown that the cumulative volume fraction of the finer sized particles is dramatically higher in pressed PBX 9501 compared to the dry blend. Experiments by Skidmore et al. [7] have shown that the consolidation of prills initially involves little damage to the large HMX crystals. As porosity is decreased, there is an increasing incidence of transgranular cracking and twinning in the large HMX crystals. If porosity is decreased to less that 1%, micro cracks grow across crystals due to crystal-to-crystal contact and intercrystalline indentation. There is contact between the fibers in PBX 9501 due to high volume fraction. In granular materials, stresses are transmitted by contact between the fibers. So, when external forces are applied to granular materials, concentration of forces in long paths, or "stress bridging" is observed.

The term "micromechanics" describes a class of methods for determining the effective material properties of composites given the material properties of the constituents. In these methods, governing equations based on continuum approximations are used to determine effective properties. The goal of micromechanics is to predict

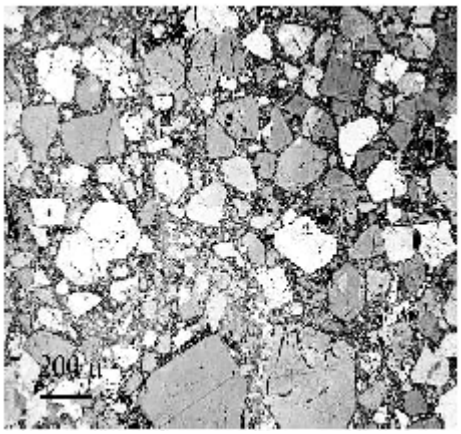

Figure 2.1. PBX9501 (adapted from [7]) pressed at ambient temperature to 2% porosity

force-displacement response of the composite. The different types of micromechanical models are analytical models, statistical models and numerical models. Micromechanical models have been used extensively since the 1960s to predict the macroscopic behavior and the effective properties of advanced composites. Extensive characteristics and capabilities of these models have already been defined. The material properties of interest in this work are the linear elastic moduli of PBXs. The high volume fraction of the dispersed component in PBXs as well as the high modulus contrast between the dispersed and the continuous components provide the main challenges. Among the many micromechanical models, the generalized method of cells (GMC) has emerged as an attractive tool to predict the elastic, inelastic, and thermoelastic behavior of a wide variety of composites. PBX 9501 microstructure is modeled using the GMC method for this research.

2.1.3 Generalized Method of Cells

One of the attractive features of GMC is its capacity to produce accurate macroscopic stress-strain responses using a relatively small number of subcells; therefore requiring very little computational effort. As a matter of fact, it has been shown by Wilt [9] that the stress-strain response of composite microstructure with circular fibers can be accurately modeled with a 7x7 subcell array. The fact that GMC is capable of

modeling relatively complex microstructures using a small number of subcells has led exclusively to implementations of the method. The method of cells (MOC) [10] and its extension, the generalized method of cells (GMC) [11] are approximate analytical methods for predicting the elastic as well as the inelastic response of fibrous composites. The methods can be used for two-dimensional (e.g., continuous fibers) or three-dimensional (e.g., short fibers or inclusions) analysis.

As in most micromechanics models, the analysis is limited to a representative volume element (RVE) that includes one fiber and the surrounding matrix material. In a typical method of cells representation, a repeating volume element consists of four rectangular subcells of which one cell is the fiber and the other cells are the matrix. The shape of the fiber does not affect the final calculations. The final results of the composite are a function of the constituent properties and fiber volume fraction. The results using this model have been shown to provide excellent correlation with numerical and experimental results. The generalized method of cells (GMC) extends the original method of cells to any number of rectangular subcells. This generalization permits improved modeling of the specific fiber shape as well as the ability to model the arrangement of fibers in the composite. Further, the inclusion of interfacial regions or graduations of properties in the fiber and matrix can be modeled. The generalized method of cells is particularly valuable for improved prediction of the inelastic response of composites. This method is extremely computationally efficient. A linear displacement field is assumed in each subcell. Small strains are assumed and the strain field in each subcell is volume averaged assuming periodic boundary conditions. The representative volume element (RVE) is discretized using a regular grid as shown in Figure 2.2.

The following is a brief summary of the main concepts associated with the GMC. Aboudi [11] has a more detailed presentation of the method. Mathematically, the generalized method of cells can be conceived to be based on the following assumptions:

1. Within each subcell, the gradient of the displacement vector is constant and equal to its value at the centroid of the subcell.

2. The entire cell can be mapped into a single point belonging to a homogeneous

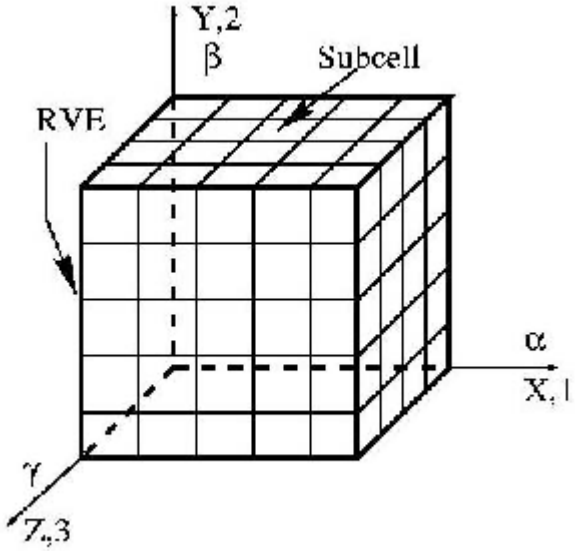

Figure 2.2. Discretization of the RVE into subcells

deformation field with displacement and displacement gradient.

This generalization permits improved modeling of the specific fiber shape as well as the ability to model the arrangement of fibers in the composite. Further, the inclusion of interfacial regions or gradations of properties in the fiber or matrix can be modeled. The generalized method of cells is particularly valuable for improved prediction of the inelastic response of composites.

2.1.4 Modeling of High Energy Composites

The major problems with modeling the composite are what should the representative volume fraction size be and what is the particle distribution. So, particles are generated randomly in the RVE based on the size distribution of the composite approximating PBX particles as spheres and cubes. Then the discretization of the RVE is done and the RVE is homogenized to perform the GMC analysis to get the results. The homogenization makes the calculation of the properties easy. The homogenization is a very important step in using GMC to model the high-energy

composites. The homogenization method is clearly explained below.

A two-step homogenization scheme is used to obtain the effective mechanical properties for the composite material. The first step is the subcell homogenization. The HMX particles in PBX 9501 are approximated to be either spheres or cylinders. Figure 2.3(a) shows the spherical and cylindrical distribution of the particles in the subcell. The total volume fraction for the subcell is calculated by adding the volume fractions of all the individual fibers. This distribution of particles is replaced with a single centrally located particle producing the same particle volume fraction for the subcell. Figure 2.3(b) shows the single spherical and cylindrical particle in the subcell with the same volume fraction. The first assumption in GMC lets us do this kind of operation. The properties for the resulting subcells are calculated and stored for the next step of homogenization. This process is repeated for each subcell within the RVE, effectively producing an array of subcells with different isotropic properties as shown in Figure 2.4.

The second stage of homogenization is performed for the entire RVE. The subcell properties calculated from the first step of homogenization are used in this step. The effective properties of the subcells are averaged to predict the effective properties of the composite material. This homogenization produces the desired set of material properties that can be used in a structural simulation. Figure 2.4 shows the second step of homogenization in which the different subcells with different properties are used to calculate the effective properties of the material.

2.2 Stress Bridging

2.2.1 What Is Stress Bridging?

The PBXs of interest to this research contain more that 90% particles by volume, so these particles are bound to have contact with other particles. To check the efficiency of GMC when particles are in contact, we have simulated a number of bridging models. In particular, when external forces are applied, concentration of forces in long paths, or "stress bridging", is observed. In granular materials, stresses are transmitted by contacts between the grains. Grains vary in size, not all grains

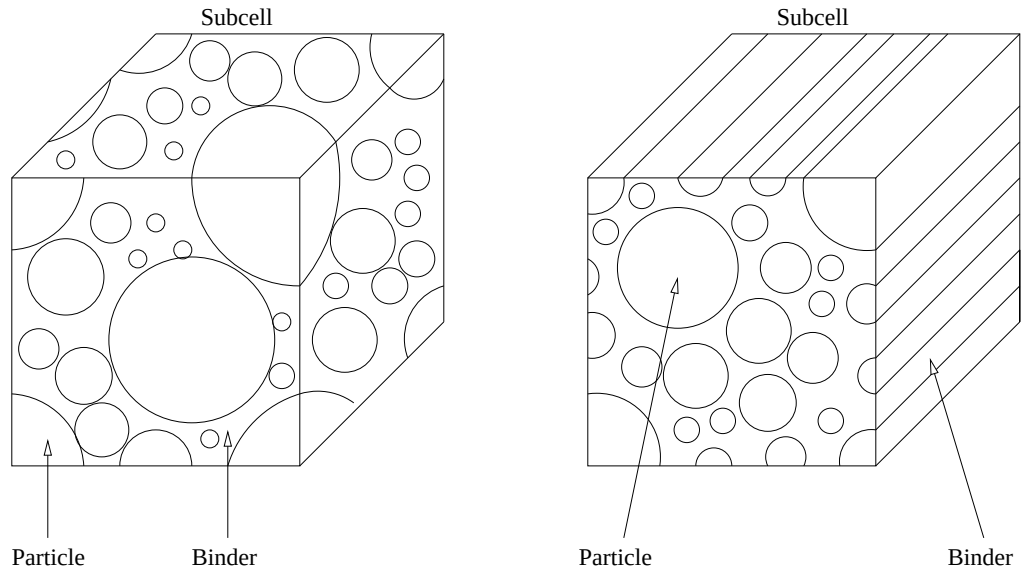

(a) Spherical, Cylindrical particles

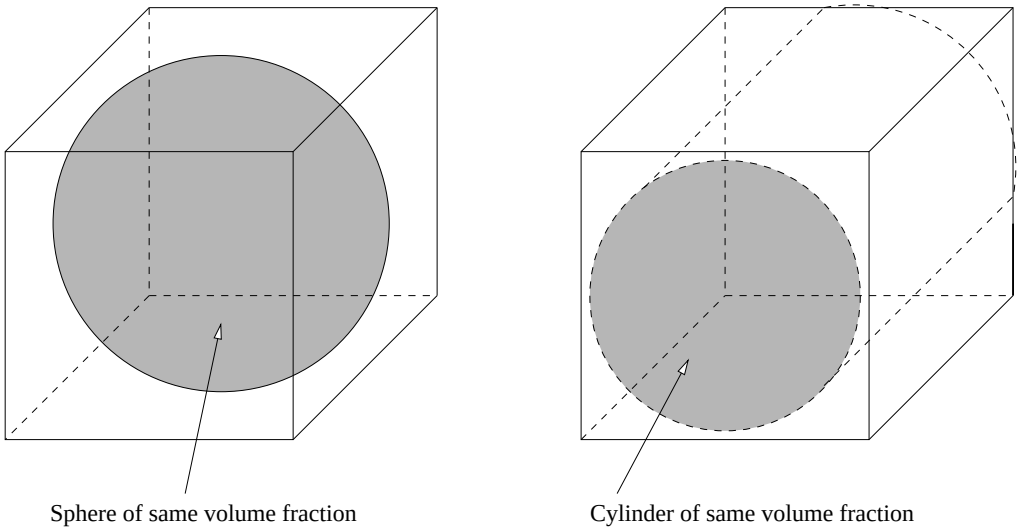

(b) After Homogenization

Figure 2.3. First step of homogenization

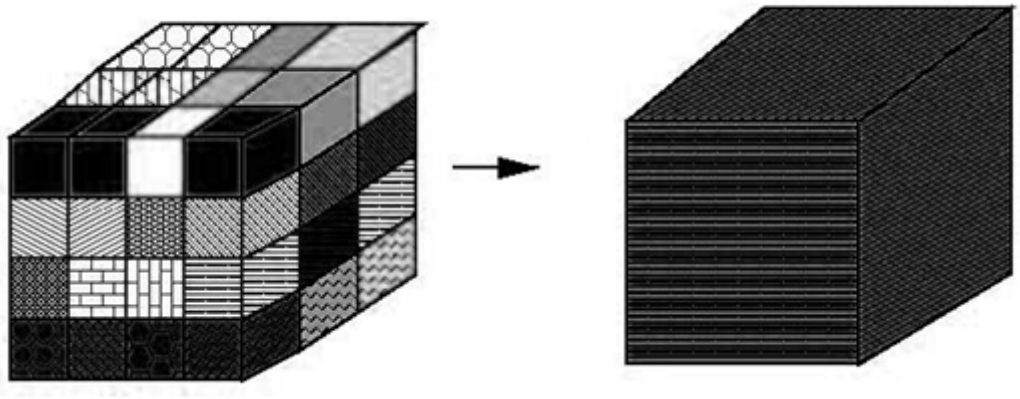

(a) Subcells with different materials (b) Homogenized RVE

Figure 2.4. Second step of homogenization

are in contact, and not all contacts are identical. Stress bridging is basically stress paths due to contact between particles in the direction of loading.

GMC has been found to accurately predict the modulus values obtained using finite element analysis for all distributions modeled. Wilt [9] showed that 1088 constant strain finite elements are required to accurately model the composite. Comparisons of effective stiffness properties predicted by GMC with finite elements have shown that GMC performs well for low modulus contrast materials with volume fraction less than 60%. GMC predicts lower effective stiffness for high contrast materials with high volume fraction. In this section GMC is applied to select models containing stress bridging paths and the predicted properties are compared to the finite element results. The goal is to demonstrate the effects of stress bridging on select models and how to improve GMC to accurately predict the properties of the material.

The stress bridging model and the nonstress bridging model are shown in Figure 2.5(a) and Figure 2.5(b). The models have the same exact volume fraction. Figure 2.5(a) shows the stress bridging path in the subcell as the particles are touching each other. The material in this case is really stiff in the vertical direction because of the contact between the fiber particles. The contact between particles causes the

particles to act like one continuous particle from the top to the bottom. Figure 2.5(b) shows the nonstress bridging model as there is no contact between the particles. The models started with the same fiber and same matrix properties. After the first step of homogenization the stress bridging model and nonstress bridging model are shown in Figure 2.6. The models have the same exact volume fraction but different effective properties to proceed to the second step of homogenization. The stress bridging model is stiffer than the nonstress bridging model. This difference changes the overall prediction of the properties. Stress bridging in the composite has to be accounted for during the first step of homogenization to predict accurately with GMC.

To validate that stress bridging has an effect on the overall properties of the material, stress bridging and the nonstress bridging approaches were modeled using the Finite Element Model (FEM). These models are shown in Figures 2.7 and 2.8. The volume fraction of both the models are very close and the geometry is similar. Figure 2.7 shows that there is significant contact between the fibers. Figure 2.8 shows that the fibers are not in contact with each other. The following boundary conditions were applied to the models to simulate multipoint boundary constraints. The bottom wall and the left wall are fixed by setting the degrees of freedom equal to zero. A strain of 0.005 is applied on the top face and the right wall nodes are coupled to move in a straight line. ANSYS software was used to analyze these models. The stress was calculated by taking into account the force on the right wall divided by the area. The elastic modulus was calculated by division of the stress and the strain. The elastic modulus calculated is listed in Table 2.3.

The results from Table 2.3 clearly show that stress bridging affects the elastic modulus in the composite by at least two orders of magnitude. In the two-step homogenization process, stress bridging modifies the properties of the subcells during the first step of homogenization. The second step of the homogenization would produce inaccurate results if stress bridging was not taken into account while calculating the composite properties during the first step. The contact between the particles can be grouped in two main categories namely linear and nonlinear contact. This research focuses on solving this problem by using these two approaches. The straight line

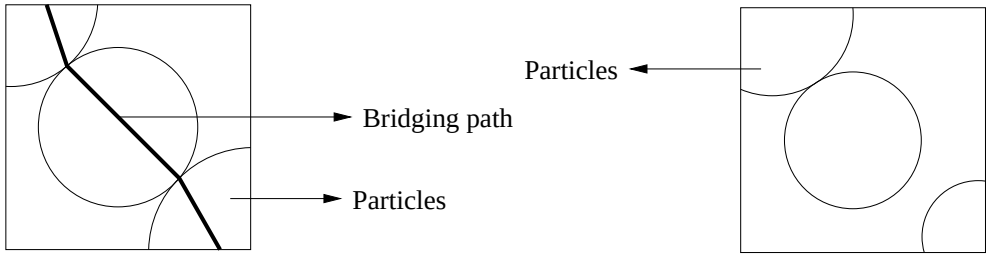

(a) Stress bridging model (b) Nonstress bridging model

Figure 2.5. Stress bridging and nonstress bridging models

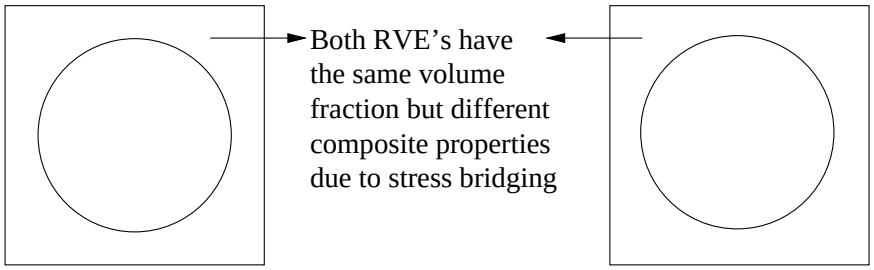

Figure 2.6. After first step of homogenization

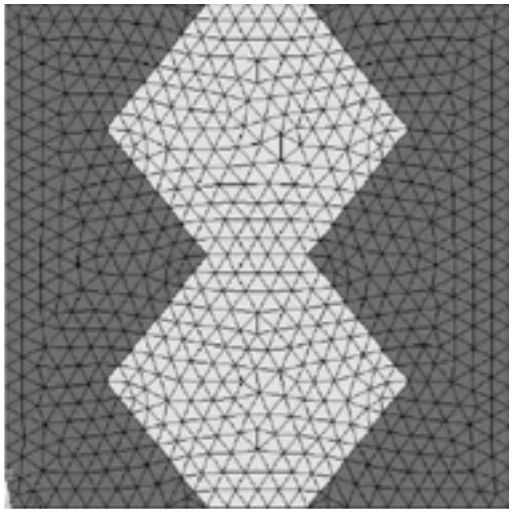

Figure 2.7. Stress bridging finite element model

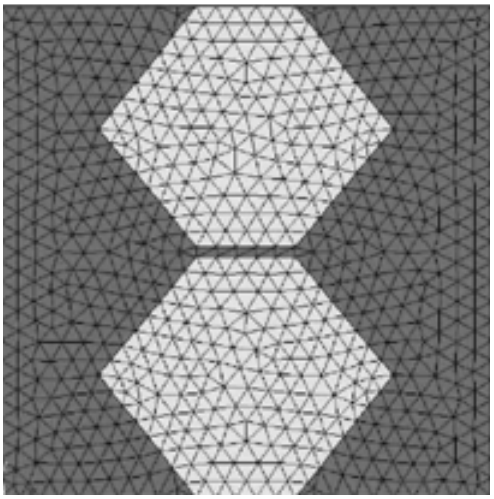

Figure 2.8. Nonstress bridging finite element model

Table 2.3. FEM results for stress bridging and nonstress bridging models

Models	Elastic Modulus (MPa)
Stress Bridging	2001.1
No Stress Bridging	29.1

approach is based on the contact of the particles in a straight line. If the particles are rectangular in nature this is the most likely contact that will be seen. The arc approach models after the cases where the particles are more cylindrical in nature. These approaches are discussed in more detail in the next section.

2.2.2 Approaches to Solve Stress Bridging

2.2.2.1 Arc Approach

The arc approach models the contact between the particles and the matrix. The arc approach can be modeled for the cylindrical particles in PBXs. The stress bridging path as seen in Figure 2.5 has to run from the top edge to the bottom edge for the elastic modulus to be different from a model that has no stress bridging. The arc approach has two submodels, namely the convex (curving out) and concave (curving in) models. Figure 2.9 shows the convex arc model and Figure 2.10 shows the concave arc model. The lighter shade in Figure 2.9 and Figure 2.10 represents the particle or the fiber and the darker shade represents the matrix. In both models the arc is drawn from the top edge to the bottom edge of the cell. The models may look the same but clearly the volume fraction of the fiber varies greatly between the convex and concave models but the contact points on the top edge and the bottom edge are identical. In general, when the arc is concave the volume fraction is below 50% and when the arc is convex the volume fraction is above 50%. Several models (convex and concave) with different volume fractions have been used to find the stress bridging parameter.

The arc approach has some drawbacks for a generalization theory. The top edge contact area, bottom edge contact area and the particle volume fraction are needed for this approach to accurately predict the properties. These three variables are not related in any way or shape, so this makes it hard to find the bridging parameter using this kind of generalization and leads us do more experimentation on the straight line approach, which is explained more in detail in the next section.

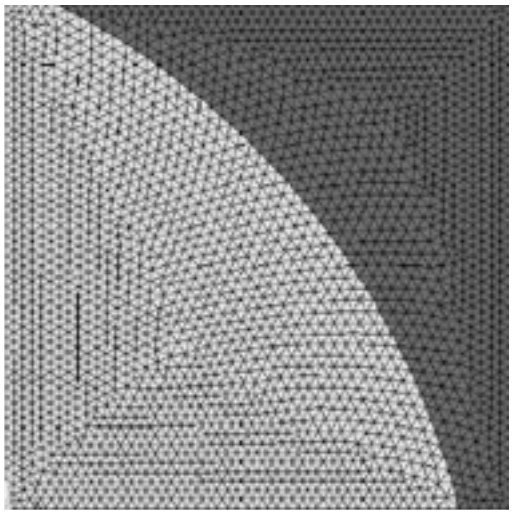

Figure 2.9. Convex arc (FEM)

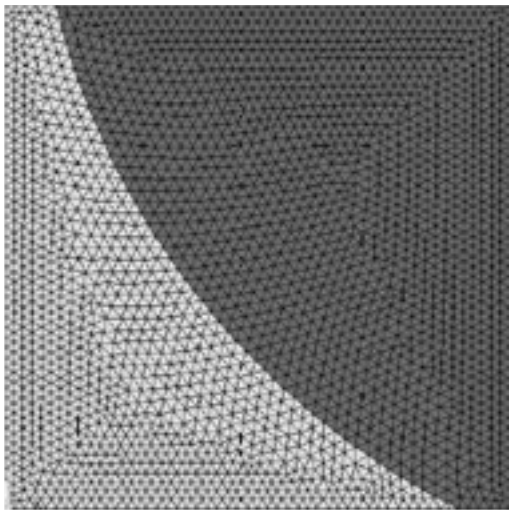

Figure 2.10. Concave arc (FEM)

2.2.2.2 Straight Line Approach

The straight line approach is very similar to the arc approach. It has the top contact area, bottom contact area and the volume fraction of the particle; however, in this approach we need only two variables instead of three. In this approach a straight line is assumed to be connecting the top and the bottom edges, so if the top contact area and bottom contact area are known, the volume fraction is fixed for that specific model. Figure 2.11 shows the straight line approach model. The top contact area of fiber is 10% and the bottom contact area is 90%, so the volume fraction of the fiber is 50%.

2.2.3 Arc Approach vs Straight Line Approach

Several straight line and arc FEM models were analyzed to see if the methods predicted different results altogether. The volume fraction for the arc approach was varied from 30% to 65%. The straight line approach volume fraction varied from 25% to 50%. The top and bottom contacts were changed between 10 to 100% for both the straight and arc approaches. A strain of 0.005 is applied on the top face of the subcell. The left edge, bottom edge are constrained from moving and the right edge is coupled to move on a straight line. Figure 2.12 shows the above described setup.

The elastic modulus for each model is calculated by dividing the stress by strain, which formulated is E = σ/ϵ where σ = stress and ϵ = strain. Stress is (F/A) where F is the force applied to the object and A is the cross sectional area through which the force is applied. Strain is δL/L where δL is the amount by which the length of the object changes and L is the original length of the object. The elastic modulus for the fiber (E) and the matrix (E_m) are calculated for each model in both approaches. The E/E_m ratio was calculated for each model and these ratios are presented for different volume fractions in Table 2.4.

Figure 2.13 graphs the values from Table 2.4 for the arc approach and the straight line approach. The E/E_m ratio is much further apart at lower volume fraction, as the volume fraction increases the values converge. They are practically the same value at 50% volume fraction. For volume fractions greater than 50%, the lines should

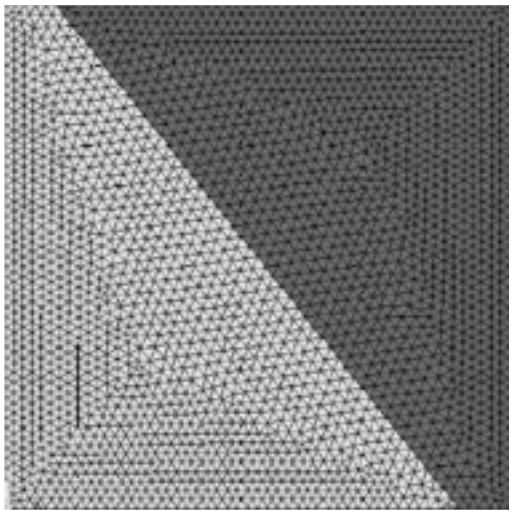

Figure 2.11. Straight line (FEM)

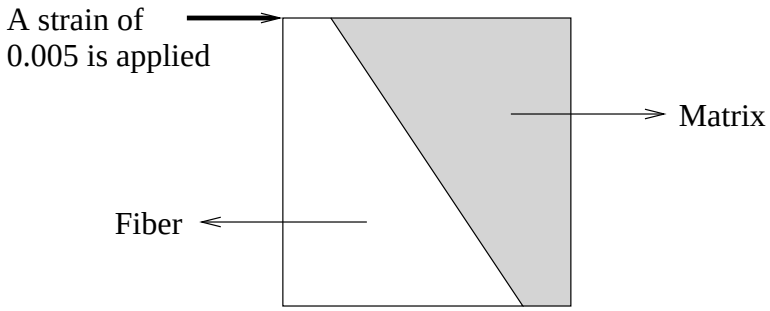

Figure 2.12. Forces on the FEM model

Table 2.4. E/E_m vs volume fraction for arc and straight line approaches.

Volume Fraction (Arc)	E/E_m (Arc)	Volume Fraction (St. Line)	E/E_m (St. Line)
31.9590	664.85	25	717.95
37.8781	782.25	30	793.60
43.2499	872.10	35	852.15
55.4237	996.30	40	896.75
62.1219	1022.55	45	930.15
		50	955.10

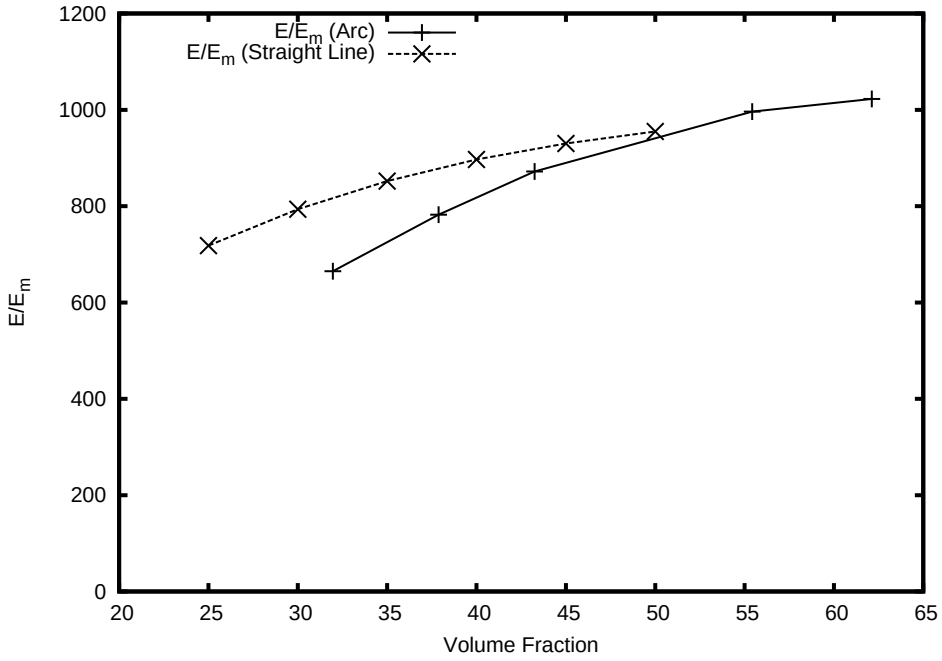

Figure 2.13. E/E_m comparison between the straight line and arc approach

follow each other very closely; hence the straight-line approach can be used as a good approximation to fit into the first homogenization step. The prediction is accurate when the volume fraction is greater than 50%. The particle volume fraction for PBXs is greater than 90% so this will be a good approach.

The straight line approach needed more data to predict the effective properties accurately. New models were generated by varying the top contact area (0% to 100%) and the bottom contact area (0% to 100%) similar to Figure 2.11. The volume fraction of the particle in the subcell was calculated from the top contact and the bottom contact areas. For example, a model was generated by fixing the top contact and then by changing the bottom contact length, resulting in different models. If the top contact is fixed at 10%, then the bottom contact can change from 0% to 100%, which would result in volume fractions of 5%-55% for this top contact case. This was repeated for top contact area of 0% to 100%. This analysis gave us 121 data points. These data points are presented in Table 2.5. These values will be applied during the first step of homogenization to account for stress bridging if present and

Table 2.5. E/E_m values for the stress bridging model.

Top Contact (%)	0	10	20	30	40	50	60	70	80	90	100
Volume Fraction (%)											
5	51.915	51.915									
10	100.585	350.9	100.585								
15	146.055	502.55	502.55	146.055							
20	187.36	622.2	700.8	622.2	187.36						
25	224.045	717.95	858.5	858.5	717.95	224.045					
30	256.145	793.6	985.95	1050.7	985.95	793.65	256.145				
35	283.83	852.15	1086.85	1209.7	1209.7	1086.85	852.2	283.83			
40	307.775	896.75	1164.45	1338.1	1400.6	1338.1	1164.45	896.75	307.775		
45	328.18	930.15	1222.55	1438.15	1559.5	1559.5	1438.15	1222.55	930.15	328.18	
50	339.865	955.1	1265.05	1513.35	1686.7	1750.5	1686.7	1513.35	1265.05	955.1	329.355
55		973.75	1295.65	1568.1	1784.2	1908.85	1908.85	1784.2	1568.1	1295.7	973.7
60			1317.6	1607.05	1856.05	2034.25	2100.4	2034.25	1856.05	1607.05	1317.6
65				1634.25	1907.35	2129.15	2258.15	2258.15	2129.15	1907.4	1634.3
70					1943.15	2198.05	2381.9	2450.3	2381.9	2198.05	1943.15
75						2246.6	2474.6	2607.5	2607.5	2474.6	2246.6
80							2541.35	2730	2800.2	2730	2541.35
85								2821.15	2957	2957	2821.15
90									3078.6	3150.1	3078.65
95										3306.65	3306.65
100											3500

then subcell properties will be calculated accordingly. Figure 2.14 represents the 3D graph of the data points from Table 2.5. The graph shows the graph between E/E_m, volume fraction and top contact.

2.3 Validation of the Method

Three different models have been taken and were validated against the stress bridging model proposed above using GMC. The first model is to validate the accuracy of the new stress bridging approach. The second model is to figure out the number of cells required to predict the properties accurately. The third model is actually modeling something close to PBX. The first two validation models have been run against 2x2, 4x4 and 8x8 subcell grids. The final model was run against 2x2, 4x4, 8x8 and 16x16 subcell grids. The models were compared to the same FEM models to validate the accuracy of the stress bridging model proposed above.

2.3.1 Simple Case Consisting of Two Particles

This is the first case for the validation of the method. The first case is divided into two smaller cases. Figure 2.15(a) is the stress bridging case, the particles touch each other causing a path to run from top of the model to the bottom through the contact point. Figure 2.15(b) is the nonstress bridging case where the particles do not touch each other; hence, there is no straight path from top of the model to the bottom of the model. The stress bridging and the nonstress bridging models have similar (not identical) geometries. The volume fraction for the stress bridging model is 45.55% fiber and the volume fraction for nonstress bridging is 41.63% fiber. The difference in volume fraction between these models is not negligible, but the effect should be pretty minimal in predicting the effective properties. The stress bridging model should produce a much higher modulus than the nonstress bridging model for very similar geometry and volume fraction. The results of this analysis are listed in Table 2.6.

Table 2.6 compares the GMC calculation of stress bridging model and the non-stress bridging model for grids (or subcells) of 2x2, 4x4 and 8x8. The values from

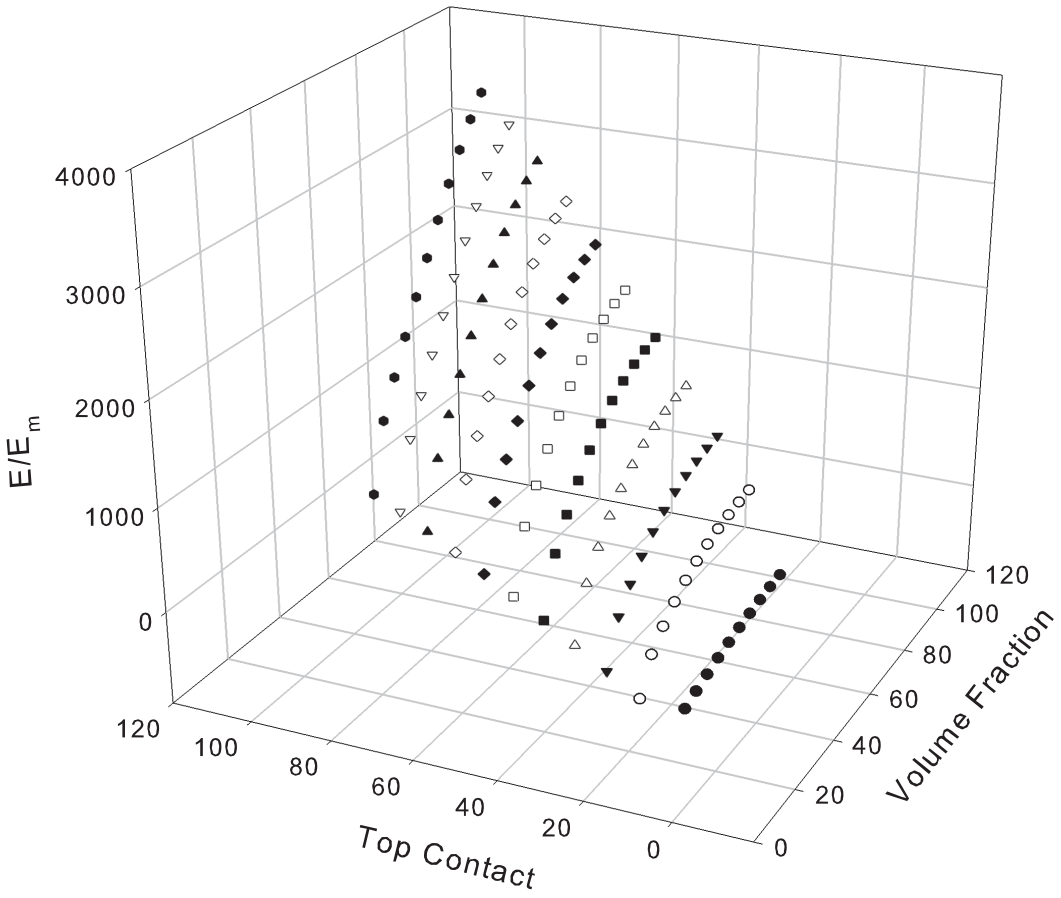

Figure 2.14. Plot between top contact vs. volume fraction vs. E/E_m for a composite material.

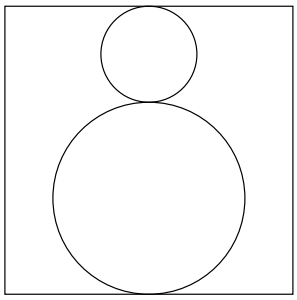

(a) Stress bridging model

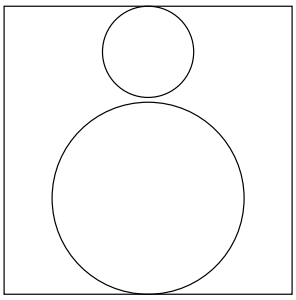

(b) Nonstress bridging model

Figure 2.15. Two particle validation model

Table 2.6. Comparison of the stress bridging vs. nonstress bridging case.

GMC Grid (Stress bridging)	E/E_m (Stress bridging)	FEM (Stress bridging)	E/E_m (Stress bridging turned off)	E/E_m (No stress bridging)	FEM (No stress bridging)
2 x 2	136.9580	137.564	3.34864	3.15830	8.0518
4 x 4	348.7401	137.564	3.12522	3.08918	8.0518
8 x 8	351.7123	137.564	3.09843	2.99784	8.0518

this calculation are then compared to the FEM calculated E/E_m and the percentage error between both approaches is calculated for each grid size. The percentage error in Table 2.6 can be attributed to two assumptions, firstly the straight line approach and secondly the E/E_m values for the volume fraction of the subcell is not a direct one to one mapping but rather an approximation of the closest values. The stress bridging model predicted similar values to non stress bridging when the GMC method ignored stress bridging in the model and this is expected because they have very similar geometry. If the stress bridging is turned off for the model, then the GMC calculation of E/E_m is highly inaccurate and hence the prediction of effective properties would be wrong.

2.3.2 GMC with Three Particles

Figure 2.16 shows the second validation model. This model has three particles that touch each other and hence there is a stress bridging path from the top to the bottom of the RVE. The primary difference between the first model and this model is that the stress bridging path is not in a simple straight line path but rather it passes through the particles and reaches the bottom. The stress path in this model presents an interesting case. This model would help in understanding how the grid size in GMC calculation affects the prediction of effective properties. The GMC analysis was done against the 2x2, 4x4 and 8x8 grids.

Figures 2.16(b), 2.16(c), 2.16(d) show the model overlayed with 2x2, 4x4 and 8x8 grids. The subcells that are marked with 'S' have stress bridging paths and need to calculated differently using GMC. The 2x2 grid has only one subcell, the 4x4 grid has five subcells and the 8x8 grid has 26 subcells with stress bridging paths. The subcells with stress bridging would equate to 25% in the 2x2 grid, 31% in the 4x4 grid and 40% in the 8x8 grid. The percentage of stress bridging increases as the grid size is increased. The GMC calculation will not be accurate as the grid size increases because more subcells calculate the stress bridging leading to higher effective properties. Wilt[9] has shown that the stress-strain response of composite microstructure with circular fibers can be accurately modeled with a 7x7 subcell array. The results of the 2x2,

4x4 and 8x8 models are listed in Table 2.7.

The results clearly indicate that the prediction of effective properties was closer for a 2x2 model than the 4x4 and 8x8 models. The 2x2 value is still not accurate but it is closer to the FEM prediction. The E/E_m is way off when GMC does not take stress bridging into account. This model proves that by increasing the grid size the E/E_m ratios are much higher due to higher percentage of stress bridging and hence resulted in higher prediction for the model.

2.3.3 GMC with Large Number of Particles

This model is a very close approximation of the actual PBX material. Figure 2.17 shows the model in detail. A regular PBX material is composed of different size particles and they fill up the subcell. The fiber volume fraction in this model is close to 80% of the total volume. This model will validate the stress bridging method proposal for GMC calculations. There is one stress bridging path from the top to the bottom between the two bigger particles on a 1x1 grid. The effective properties of this model were calculated against the 2x2, 4x4, 8x8 and 16x16 grid sizes as shown in Figures 2.18(a), 2.18(b), 2.18(c) and 2.18(d). The subcells that have been marked with a 'S' have stress bridging paths. Figure 2.18(d) was not marked this way to make it more readable. This model was then analyzed using FEM. The results of this comparison are shown in Table 2.8.

The results from Table 2.8 clearly show that the predictions using stress bridging in GMC are much closer to the predicted FEM E/E_m ratios for all grid sizes than the ones with no stress bridging. This model has predicted better results than previous models. This primarily can be attributed to the higher fiber volume fraction in this model compared to previous models. The previous models had a volume fraction less than 50%. Table 2.8 shows that if the stress bridging is not accounted for in the GMC calculations, then the E/E_m ratios are inaccurate. The E/E_m ratio when stress bridging turned off is 11.4737. The actual E/E_m ratio for the model is 332.448 and hence GMC would have predicted much lower effective properties than the actual model. The grid size also played a significant role in the accurate prediction. The

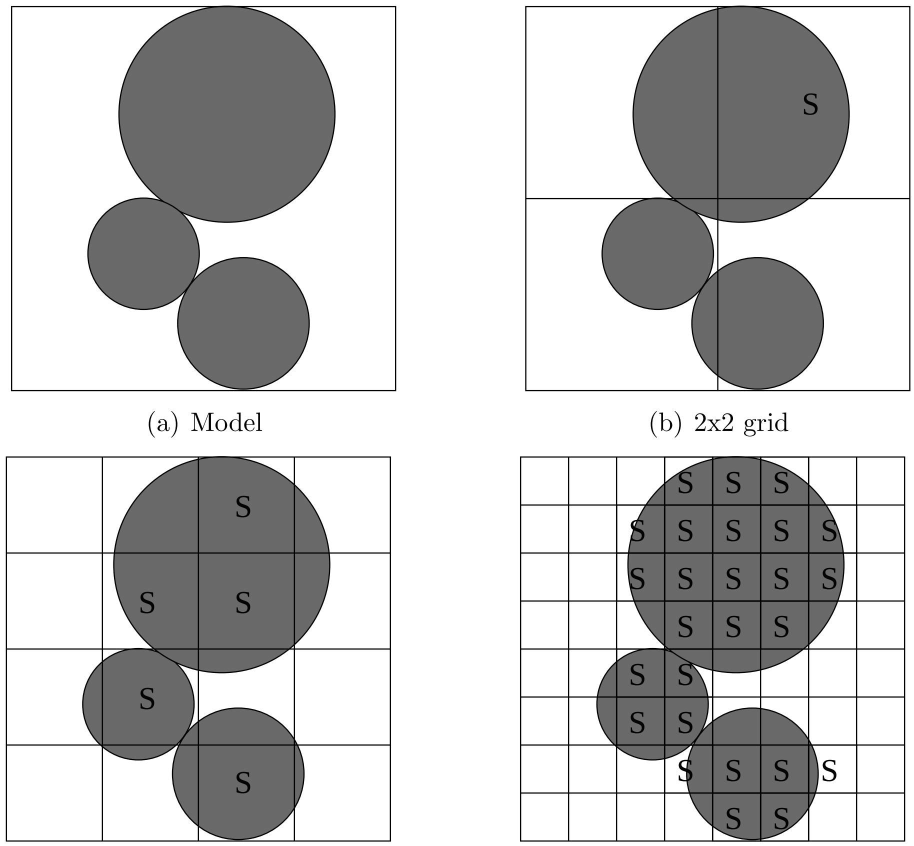

(a) Model (b) 2x2 grid (c) 4x4 grid (d) 8x8 grid

Figure 2.16. Three particles validation model

Table 2.7. Results of the second validation case against 2x2, 4x4 and 8x8.

GMC Grid	E/E_m (GMC)	FEM	E/E_m (Stress bridging turned off in GMC)
2 x 2	70.0982	26.349	2.47794
4 x 4	274.7631	26.349	2.47794
8 x 8	304.6658	26.349	2.47794

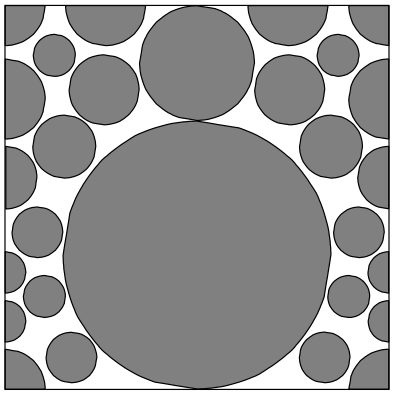

Figure 2.17. Model close to actual PBX HMX material

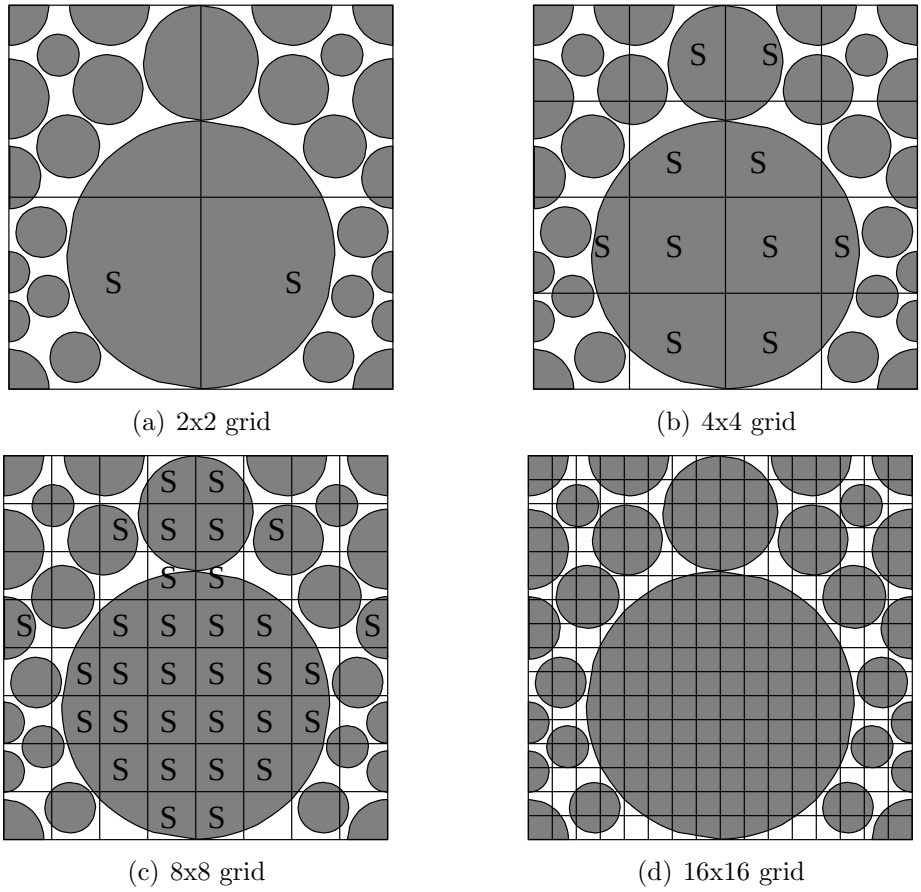

(a) 2x2 grid

(b) 4x4 grid

(c) 8x8 grid

(d) 16x16 grid

Figure 2.18. Grids for PBX HMX material validation model

Table 2.8. Results of the final validation case.

GMC Grid	E/E_m (GMC)	FEM	E/E_m (Stress bridging turned off in GMC)
2 x 2	394.496	332.448	11.4737
4 x 4	370.604	332.448	11.4737
8 x 8	352.104	332.448	11.4737
16 x 16	327.335	332.448	11.4737

2x2 grid from the results is too small to get a meaningful calculation. The 4x4 has lesser deviation but not as good as the 8x8 and 16x16 grid calculations. This research agrees with Wilt [9] that at least a 7x7 subcell array is needed for GMC calculations.

2.4 Summary and Conclusions

The PBX's materials have high volume fraction (>90%) of HMX crystals. This high volume fraction causes particle to rub against each other and when this happens the stress is transferred from one particle to another particle, creating a stress bridging path. These stress bridging paths lead to a stiffer material. GMC is a technique in micromechanics to effectively calculate the properties by dividing the particle into smaller subcells and calculating each individual subcell's properties and then the whole model.

This research focused on seeing if the GMC calculation was negatively affected in stress bridging scenarios. Table 2.3 shows that the stress bridging does exist and if not considered in GMC calculations can predict effective properties inaccurately. This investigation was to identify appropriate solution to account for stress bridging in the calculation of effective properties using GMC. Two approaches, the straight line and the arc approach, were considered and the straight line approach was picked for the ease of modeling. The straight line approach also predicted with the same accuracy as the arc approach. Several models were analyzed to come up with the data points for the straight line approach. These data are in Table 2.5.

Three unique models were analyzed to see how this model faired in the GMC calculations. These models were validated against FEM models. Grid sizes of 2x2,

4x4 and 8x8 grid were analyzed for all models. The last model was also analyzed against a 16x16 grid as it the closest model to represent PBX material.

These validation cases prove that GMC needs to account for stress bridging and a subcell array of 8x8 is the best grid size for predicting the effective properties. The higher the volume fraction, the better GMC with stress bridging predicted the properties. The first two cases had a lower volume fraction than the last model. This approach needs to complement GMC for an accurate prediction of effective properties.

2.5 References

[1] D. M. Hoffman and L. E. Caley, "Dynamic mechanical and molecular weight measurements on polymer bonded explosives from thermally accelerated aging tests I. Fluoropolymer binders," *Organic Coatings and Plastics Chemistry*, vol. 44, pp. 680–685, 1981.

[2] T. R. Gibbs and A. Popolato, *LASL Explosive Property Data*. Berkeley, California: Univ. of California Press, 1980.

[3] P. J. Rae, H. T. Goldrein, S. J. P. Palmer, J. E. Field, and A. L. Lewis, "Studies of the failure mechanisms of polymer-bonded explosives by high resolution Moire interferometry and environmental scanning electron microscopy," in *Proc. , 11th International Detonation Symposium*, (Snowmass, Colorado), pp. 66–75, 1998.

[4] G. T. Gray III, D. J. Idar, W. R. Blumenthal, C. M. Cady, and P. D. Peterson, "High- and low-strain rate compression properties of several energetic material composites as a function of strain rate and temperature," in *Proc. , 11th International Detonation Symposium*, (Snowmass, Colorado), pp. 76–84, 1998.

[5] J. J. Dick, A. R. Martinez, and R. X. Hixson, "Plane impact response of PBX 9501 and its components below 2 GPa," Report LA-13426-MS, Los Alamos National Laboratory, New Mexico, 1998.

[6] J. M. McAfee, C. B. Skidmore, G. S. Cunningham, and H. A. Nelson, "Explosive morphology from fractal analysis of micrographs," in *Proc. , 11th International Detonation Symposium*, (Snowmass, Colorado), pp. 391–398, 1998.

[7] C. B. Skidmore, D. S. Phillips, P. M. Howe, J. T. Mang, and J. A. Romero, "The evolution of microstructural changes in pressed HMX explosives," in *Proc. , 11th International Detonation Symposium*, (Snowmass, Colorado), pp. 556–564, 1998.

[8] C. B. Skidmore, D. S. Phillips, S. F. Son, and B. W. Asay, "Characterization of HMX particles in PBX 9501," in *Proc. , 10th APS Topical Conference on Shock Compression of Condensed Matter*, (Los Alamos, New Mexico), pp. 112–119, American Physical Society, 1997.

[9] T. E. Wilt, "On the finite element implementation of the generalized method of cells micromechanics constitutive model," Tech. Rep. NASA-CR-195451, National Aeronautics and Space Administration, Lewis Research Center, USA, 1995.

[10] J. Aboudi, "Micromechanical analysis of composites by the method of cells - update," *Appl. Mech. Rev*, vol. 49, no. 10, pp. S83–S91, 1996.

[11] M. Paley and J. Aboudi, "Micromechanical analysis of composites by the generalized cells model," *Mechanics of Materials*, vol. 14, pp. 127–139, 1992.

CHAPTER 3

EVALUATION OF G_{23} USING FINITE ELEMENT METHOD IN UNIDIRECTIONAL COMPOSITES

3.1 Introduction

Micromechanics is the study of composite material behavior where the interaction of constituent material is examined in detail and used to predict and define the behavior of the heterogeneous composite material. Such analyses typically assume that the fundamental material properties of the constituents are known initially. The composite material properties can be determined experimentally by testing actual composite specimens. However, in recent years, more and more attention has been given to the development of the analytical and numerical models for predicting composite material properties from the properties of the constituent materials and their relationship to each other.

A basic notion in micromechanics is the Representative Volume Element (RVE). This is a volume, that is small enough from a macroscopic point of view and could be thus treated as a typical point of the heterogeneous continuum under study. On the other hand, it should be large enough in the microscopic scale, in order to contain a large number of single inhomogeneities and therefore to be indeed representative for the microstructure of the solid. A more detailed discussion of RVEs, together with certain criteria on how to identify them, can be found in the book by Nemat-Nasser and Horis [1].

In discussing the mechanics of unidirectional composite materials, it is convenient to use an orthogonal coordinate system that has one axis aligned with the fiber direc-

tion. Figure 3.1 illustrates the orientation of the coordinate system. The transverse shear modulus (G_{23}) is calculated when the unit cell or the RVE is subjected to shear stress, or strain in the 2-3 plane. Figure 3.1 shows the ideal RVE for the square packed array of fibers.

Hill [2] and Hashin [3] proposed the concept of elastic moduli of heterogeneous materials, which was considered by studying a representative volume of the composite over whose surface the displacement and traction are uniform. The elastic moduli, which is also called the effective moduli, has been defined with the average stress and average strain.

One of the earliest micromechanics models of composite materials considered a single infinitely long fiber surrounded by matrix (RVE in Figure 3.1). The force was applied at the fiber ends, so the load transfer occurs at the end of the fiber. However, because the length of most fibers is several hundred times greater than their diameter, the region of stress transfer into the fiber from the matrix is so small that an infinite-length fiber model can be justified. Laws and Mclauglin [4] investigated the fiber length effect on the overall properties of composite materials with the application of the self-consistent method and compared the results with experimental results using fibers of same length. However, the comparison was only for the Young's modulus.

Adams and Doner [5, 6] were among the first to use finite difference analysis on the composite RVE to find the properties of the composite. These were two-dimensional approximations for an array of fibers in a matrix. Our approach is to analyze the composite material for transverse shear modulus (G_{23}) using the finite element method and to compare to other methods in the literature.

Figure 3.2 is an extension of the RVE in Figure 3.1 RVE. Both figures show a fibrous composite with a cylindrical fiber running along the one axis. We see the cross sectional area of the material in the Figure 3.2. Uniform displacements or strain are applied to the RVE's boundaries with outward normals in the two directions as shown in Figure 3.2 to calculate E_2.

The finite element method is commonly used to calculate the effective transverse modulus E_2 as it is straightforward to identify the RVE and the boundary conditions

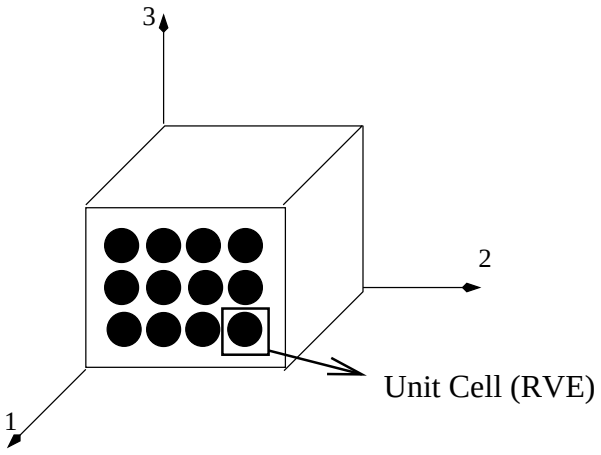

Figure 3.1. Coordinate system

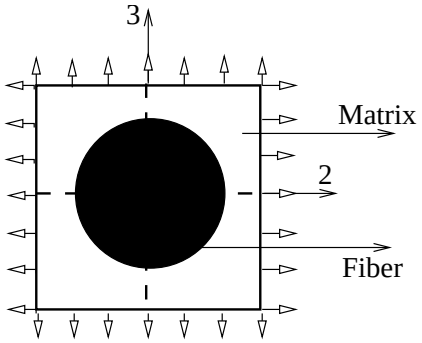

Figure 3.2. Unit cell (RVE) from Figure 3.1

to apply to the boundaries of the RVE. However, there are challenges associated with the selection of the RVE for the calculation of G_{23}, which are explained in detail in the following paragraphs.

The finite element method has been known to produce accurate results when an appropriate number of finite elements are used. To model the RVE shown in Figure 3.2, one can model a quarter section and use symmetry boundary conditions to get the end result for the whole unit cell shown in Figure 3.2. This quarter section RVE used for finite element modeling is shown in Figure 3.3.

Next consider the RVE under shear strain or uniform shear displacements on the boundaries of the RVE as shown in Figure 3.4(a). The RVE after the shear strains are applied would look like that shown in Figure 3.4(b).

To calculate the transverse shear modulus (G_{23}) for the unidirectional composite in Figure 3.1, one may be tempted to consider the approach shown in Figure 3.4. Figure 3.5 shows the results of this approach. Using the quarter section model, the unit cell is broken into four different parts and the unit cell is no longer a continuous region.

Figure 3.5(b) shows that we would get inaccurate results for shear modulus if we proceed with the straight approach of applying shear forces on the quarter section RVE as shown in Figure 3.3. The solution to this problem of identifying a RVE and applying correct boundary conditions to calculate the transverse shear modulus is presented in the following sections.

3.2 Solution Technique

The objectives of this research are first to develop a modeling approach using the finite element method to calculate the transverse shear modulus (G_{23}) of a unidirectional composite material and secondly to compare the results with those from classical micromechanics theory and other methods.

The focus is to identify a RVE and employ the finite element method to model a plane normal to the fiber axis. In this plane, assuming generalized plane strain, the material properties of the fiber and matrix are used to calculate the shear modulus

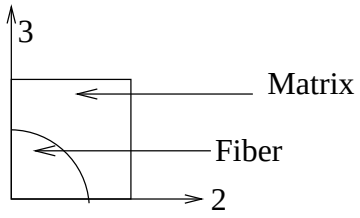

Figure 3.3. The quarter section RVE to be used in finite element modeling

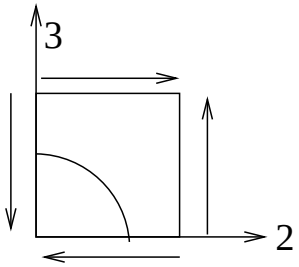

(a) Constant uniform displacement on the boundaries of the RVE

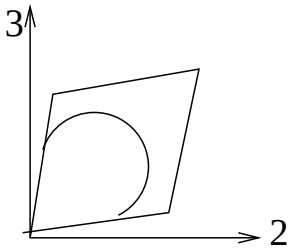

(b) Deformation results after the boundary conditions are applied

Figure 3.4. The quarter section RVE under transverse shear loading

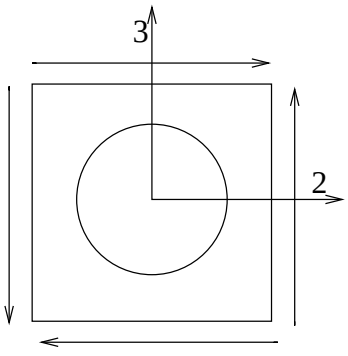

(a) Loading conditions for the unit cell

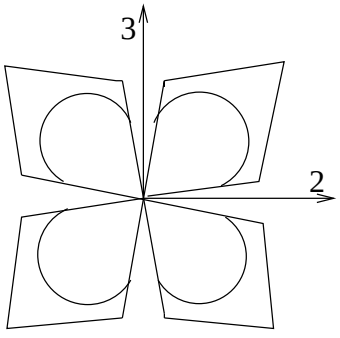

(b) Results of the loading conditions on the unit cell

Figure 3.5. Unit Cell (RVE) under transverse shear loading

G_{23}. The following section presents the modeling approach.

Figure 3.6 shows the cross section of the composite from Figure 3.1 rotated at 45 degrees to the 2-3 plane with shear strain being applied on the composite as shown by the arrows. The dark square shown in the figure is the RVE to be used for calculating G_{23}. The RVE is being stressed in two directions in the 2-3 plane, a condition known as equivalent biaxial loading.

With biaxial loading conditions on the RVE, we can specify the new boundary conditions to be applied on the RVE as shown in Figure 3.7. With all the boundary conditions specified, the transverse shear modulus (G_{23}) can be calculated from the average shear stress and shear strain applied on 2-3 plane. A constant displacement has been applied on the boundaries of the RVE.

The solution to accurately modeling a RVE for calculating G_{23} is summarized in Figure 3.8. In this figure the RVE is under shear strain loading. In Figure 3.8(b) the RVE is under tension and compression strains on the boundaries of the RVE or the biaxial loading on the RVE. Both these loading conditions should give us the same result for the transverse shear modulus; however, it is easier to model the boundary conditions shown in Figure 3.8(b) for finite element analysis.

The finite element code ANSYS® Academic Research, Release 5.5 was used for analyzing the models. A two-dimensional six-node triangular structural solid element was used in finite element model. This element is well suited for an irregular mesh. The volume fraction of the fiber in the RVE was varied from 0.04 to 0.78 for the models. The models were analyzed for carbon/epoxy and glass/epoxy composite materials. The elastic properties used for the matrix and the fibers modeled are listed in Table 3.1.

The finite element mesh model that was used for the computation of G_{23} is shown in Figure 3.9. The volume fraction for this case is 0.40. The light areas in the figure are the fibers and the darker areas represent the matrix. The volume fraction was varied from 0.04 to 0.78. (A circle in a rectangle can have only a maximum area of 0.78.)

A displacement δ was applied on the faces of the RVE. Tension strain was applied

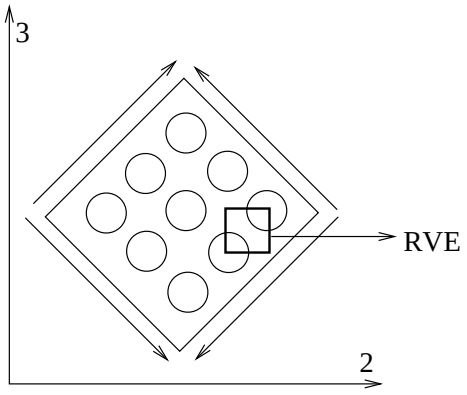

Figure 3.6. Cross section of array

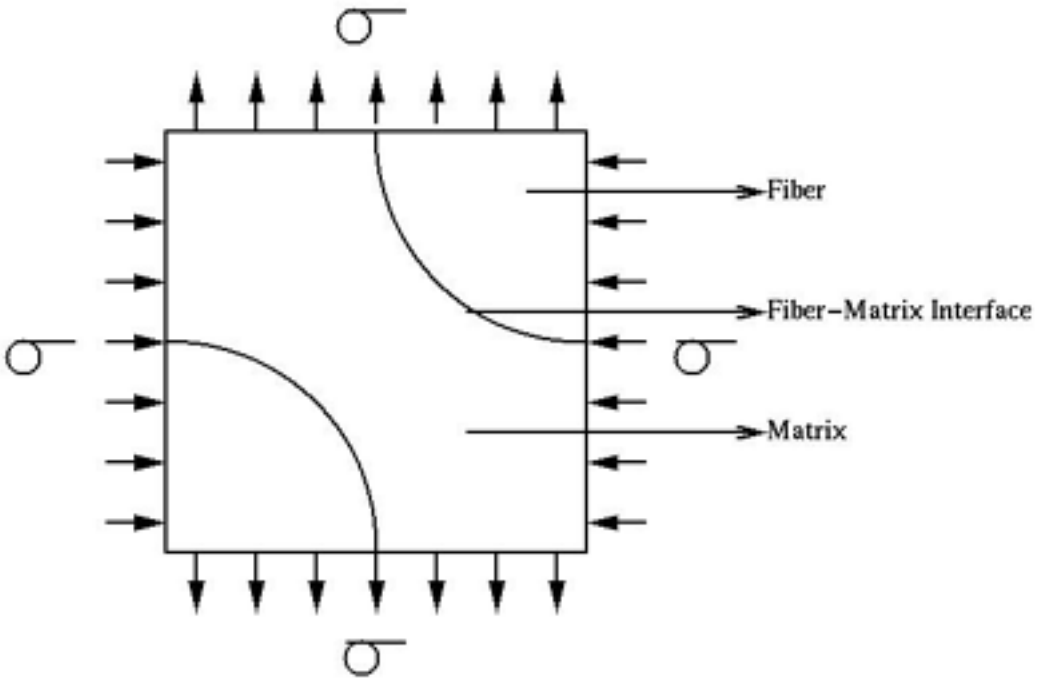

Figure 3.7. Representative Volume Element (RVE) and applied boundary conditions

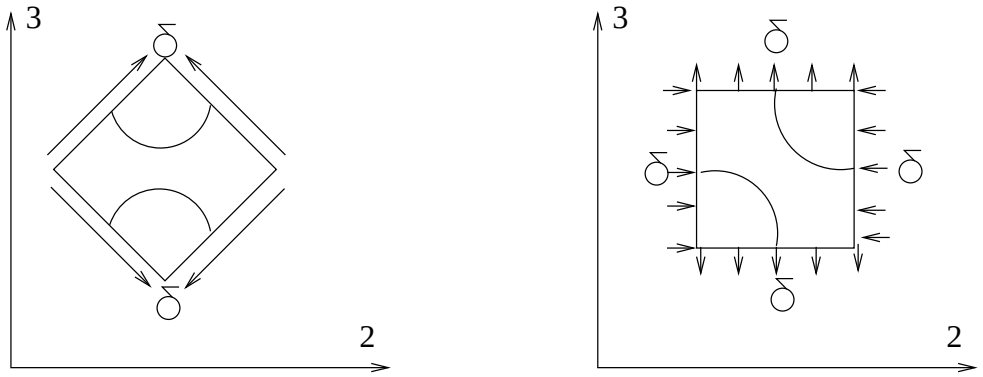

(a) The RVE under shear strain loading

(b) The RVE under tension and compression

Figure 3.8. The RVE and boundary conditions for calculation of G_{23}

Table 3.1. Fiber and matrix properties for glass and carbon

Property	Carbon	Glass	Epoxy
E_A (GPa)	232	113.4	5.35
E_T (GPa)	15	113.4	5.35
G_A (GPa)	5.02	46.5	1.98
G_T (GPa)	24	46.5	1.98
n_{12},n_{13}	0.28	0.22	0.35

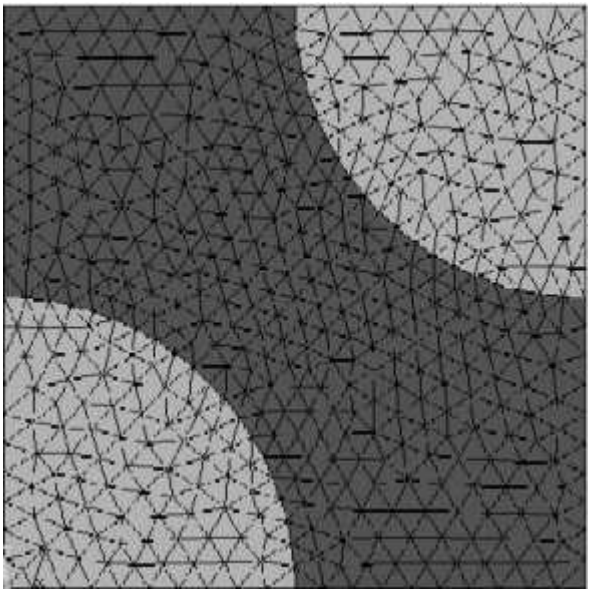

Figure 3.9. Finite element mesh for volume fraction of 0.04

on the horizontal faces and compression strain on the vertical faces. The applied strains make RVE's deforming exactly the same manner as the composite would deform under transverse shear loading. To be more specific, the following boundary conditions were imposed on the models to simulate the multipoint boundary constraints. A unit displacement $+\delta$ was applied on the left face (0,y), -δ was applied on the right face (L, y), -δ was applied on the bottom face (x, 0) and + δ was applied on the top face (x, L). Figure 3.8(b) shows the boundary conditions applied to the RVE.

The transverse shear modulus is defined as $G_{23} = \tau_{23}/\gamma_{23}$ where τ_{23} is the shear stress in the 2-3 plane and γ_{23} is the shear strain in the 2-3 plane. There are tension and compression strains in the boundary conditions applied to the RVE, so the shear strain γ_{23} is 2ϵ and ϵ is 2δ by adding the unit displacements along the horizontal faces or vertical faces as shown in Figure 3.8(b). The finite element models used a strain (2δ) of 0.01 along the horizontal and vertical faces.

To calculate the shear stress τ_{23} from the finite element model, the nodes on the top surface are selected, the forces on these nodes are summed and the total force is calculated. This force divided by the area of the top surface to produce the shear stress τ_{23}. The transverse shear modulus is then computed and the results of this investigation are compared with classical micromechanics solutions.

3.3 Results and Discussion

The materials used for the investigation are carbon/epoxy and glass/epoxy composites. The volume fraction of the fiber was varied from 0.04 to 0.78 in the RVE models. The RVE is then subjected to a tensional strain and compressional strain of 0.01. Table 3.1 shows that the G_{23} for glass composite with no epoxy is 46.5 GPa and for carbon with no epoxy is 5.02 GPa.

The results of these analysis have been compared to other classical solutions. Herakovich's [7] book explains these classical solutions in more detail. The results of this investigation are compared with Voigt's approximation, Reuss's Approximation, Self-Consistent, Mori-Tanaka and Generalized Method of Cells (GMC) solutions.

The Voigt approximation method assumes that the strains are constant throughout the composite. The Reuss approximation method assumes that the stresses were constant throughout the composite. The Voigt and Reuss solutions are generally known as the upper and lower bounds of the solutions and hence are not regarded as accurate solutions compared to solutions developed later. The Self-Consistent method is based on the solution to an auxiliary inclusion problem where a single ellipsoidal inclusion is embedded in an infinite medium. Uniform stresses or strains are applied at infinity with the objective of determining the stresses and strains in the inclusion. The Mori-Tanaka solution basically is the fourth order tensor that relates average inclusion strain to average matrix strain and approximately accounts for fiber interaction effects. The Generalized Method of Cells (GMC) is an approximate analytical method for predicting the elastic as well as inelastic response of fibrous composites.

All results have been plotted to investigate how closely the finite element solution models the transverse shear modulus when compared against the other classical approaches.

3.3.1 Glass/Epoxy

Table 3.2 shows the transverse shear modulus G_{23} results for glass/epoxy composite. As shown in the table, the volume fraction of the fiber was varied between 0 and 0.77 to calculate the shear modulus for the glass/epoxy composite.

Figure 3.10 compares the results of the finite element model to the classical solutions to investigate the accuracy of the finite element method for calculating the transverse shear modulus (G_{23}) for a glass/epoxy composite. The finite element solution falls between the upper and lower bounds of the solutions. Figure 3.10 shows that the finite element solution is in between the Mori-Tanaka and GMC solutions. This clearly shows that the model used for calculating G_{23} in this research produces similar results compared to other micromechanics solutions.

Table 3.2. Results of G_{23} calculation for glass/epoxy composite

Volume Fraction (fiber)	Volume Fraction (matrix)	G_{23} (GPa)
0.000	1.000	2.075
0.040	0.960	2.193
0.098	0.902	2.366
0.204	0.796	2.710
0.304	0.696	3.098
0.392	0.608	3.523
0.501	0.499	4.249
0.604	0.396	5.368
0.705	0.295	7.736
0.770	0.230	12.690

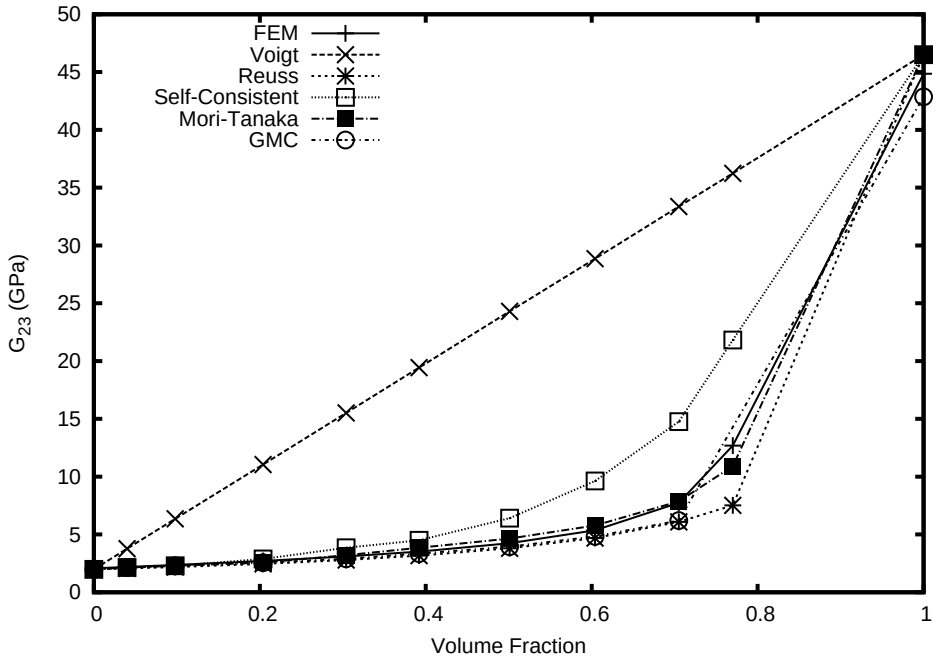

Figure 3.10. Transverse shear modulus (G_{23}) for glass/epoxy with other classical solutions.

3.3.2 Carbon/Epoxy

The same finite element models used for glass/epoxy composite were used for the the carbon/epoxy composite with one exception of the material properties. The carbon/epoxy material properties were used for this analysis. Table 3.3 shows the transverse shear modulus G_{23} results for carbon/epoxy composite. The volume fraction of the fiber was varied from 0.04 to 0.78 for the results.

Figure 3.11 compares the results of the finite element solution to the classical solutions. This comparison is done to see the accuracy of the finite element solution for transverse shear modulus (G_{23}) calculation. The finite element solution for carbon/epoxy composite just like the glass/epoxy composite falls between the upper and lower bounds of the solutions. The finite element solution in the carbon/epoxy composite case is predicting a little higher values than the classical solutions like Self-Consistent, Mori-Tanaka and GMC but the trend is very similar to these solutions.

3.4 Conclusions

This investigation focussed on the calculation of the transverse shear modulus (G_{23}) of unidirectional composites using the finite element method. The investigation included identifying appropriate boundary conditions to be applied to the identified Representative Volume Element (RVE). After identifying the boundary loading conditions and running the element models using commercial finite element analysis software, results were compared to other classical solutions. The finite element results for glass/epoxy and carbon/epoxy composites compared well against classical solutions like Self-Consistent, Mori-Tanaka and Generalized Method of Cells (GMC). The results suggest that the finite element model may be used to predict transverse shear modulus (G_{23}) for unidirectional composites.

Table 3.3. Results of G_{23} calculation for carbon/epoxy composite

Volume Fraction (fiber)	Volume Fraction (matrix)	G_{23} (GPa)
0.040	0.960	2.144
0.098	0.902	2.244
0.204	0.796	2.435
0.304	0.696	2.635
0.392	0.608	2.833
0.501	0.499	3.120
0.604	0.396	3.461
0.705	0.295	3.910
0.770	0.230	4.303

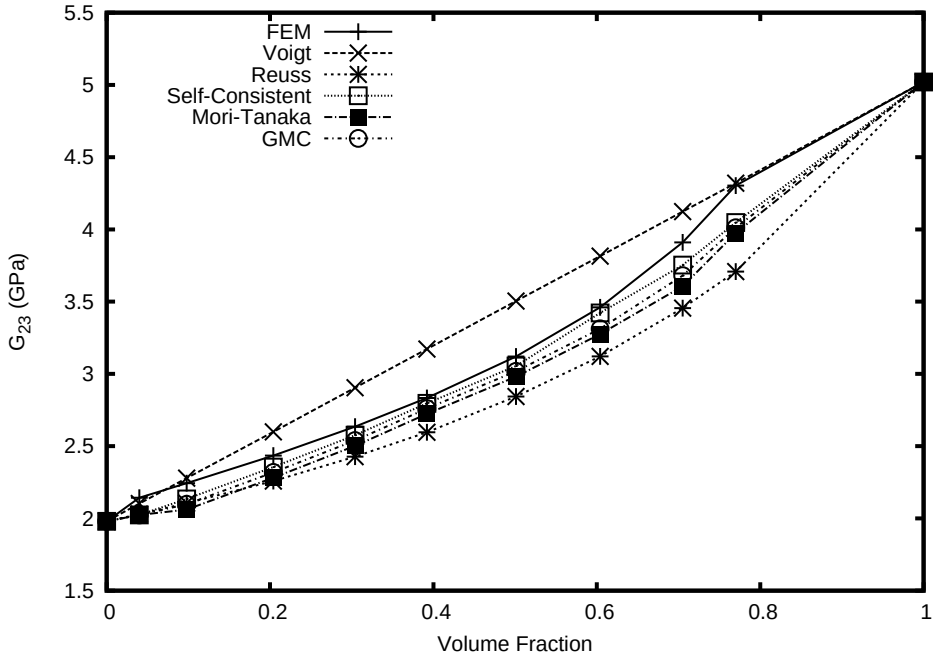

Figure 3.11. Transverse shear modulus (G_{23}) for carbon/epoxy with other classical solutions.

3.5 References

[1] S. Nemat-Nasser and M. Hori, *Micromechanics : Overall Properties of Heterogeneous Materials*. Amsterdam: North-Holland, 1993.

[2] R. Hill, "Elastic properties of reinforced solids : some theoretical principles," *J. Mech. Phys. Solids*, vol. 11, pp. 357–372, 1963.

[3] Z. Hashin, "Theory of mechanical behaviour of heterogeneous media," *Applied Mech. reviews*, vol. 17, pp. 1–9, 1964.

[4] N. Laws and R. McLaughlin, "The effect of fiber length on the overall moduli of composite materials," *Journal of the Mechanics and Physics of Solids*, vol. 27, pp. 1–13, 1979.

[5] D. F. Adams and D. F. Doner, "Transverse normal loading of a unidirectional composite," *J. Composite Materials*, vol. 1, pp. 152–164, 1967.

[6] D. F. Adams and D. F. Doner, "Longitudinal shear loading of a unidirectional composite," *J. Composite Materials*, vol. 1, pp. 4–17, 1967.

[7] C. T. Herakovich, *Mechanics of Fibrous Composites*. Wiley, 1998.

CHAPTER 4

RECOMMENDATIONS

4.1 Introduction

This research addressed two key aspects within the general topic of micromechanics for numerical prediction of composite properties. The stress bridging model was developed so the generalized method of cells could predict much more accurate effective properties of the composite. The transverse shear modulus G_{23} model identified a representative volume element (RVE) and applied boundary conditions to effectively predict the values. The need for these techniques has been established through investigation into the effect of stress bridging and G_{23} calculation.

4.2 Recommendations for Future Work

This research focused on the stress bridging effects in high energy materials and its incorporation into the generalized method of cell (GMC) solution and calculating G_{23} in unidirectional composites. The recommendations are organized in the same order in the following subsections.

4.2.1 Stress Bridging in Particulate Composites

This research used the straight line approach for the GMC calculations. Future work would involve modeling the arc approach into the GMC. The arc approach will be hard to map but may be more accurate when compared to the straight line approach. This research focused on the cylindrical particles. Future research can model other geometric fiber shapes to determine the stress bridging effects in polymer bonded explosives (PBXs). This research focused on a two-dimensional plane. Future research can include the three-dimensional models for better prediction of effective properties when stress paths are present in the composite model.

4.2.2 Calculation of G_{23} in Unidirectional Composites

This research primarily focused on calculating only the transverse shear modulus G_{23}. Future research can involve identifying the representative volume element (RVE) and boundary conditions for other properties along the 2-3 plane using a solution similar to that used to calculate the G_{23}.